

This is a repository copy of *NEDA—NEutron Detector Array*.

White Rose Research Online URL for this paper:

<https://eprints.whiterose.ac.uk/144728/>

Version: Accepted Version

---

**Article:**

Valiente-Dobón, J. J., Jaworski, G., Goasduff, A. et al. (56 more authors) (2019) *NEDA—NEutron Detector Array*. *Nuclear Instruments and Methods in Physics Research, Section A: Accelerators, Spectrometers, Detectors and Associated Equipment*. pp. 81-86. ISSN 0168-9002

<https://doi.org/10.1016/j.nima.2019.02.021>

---

**Reuse**

This article is distributed under the terms of the Creative Commons Attribution-NonCommercial-NoDerivs (CC BY-NC-ND) licence. This licence only allows you to download this work and share it with others as long as you credit the authors, but you can't change the article in any way or use it commercially. More information and the full terms of the licence here: <https://creativecommons.org/licenses/>

**Takedown**

If you consider content in White Rose Research Online to be in breach of UK law, please notify us by emailing [eprints@whiterose.ac.uk](mailto:eprints@whiterose.ac.uk) including the URL of the record and the reason for the withdrawal request.

# NEDA - NEutron Detector Array

J.J. Valiente-Dobón<sup>a</sup>, G. Jaworski<sup>a</sup>, A. Goasduff<sup>a,b,c</sup>, F.J. Egea<sup>a,b,c,d</sup>,  
V. Modamio<sup>a,e</sup>, T. Hüyük<sup>d</sup>, A. Triossi<sup>b,c,f</sup>, M. Jastrząb<sup>g</sup>, P.A. Söderström<sup>h</sup>,  
A. Di Nitto<sup>i</sup>, G. de Angelis<sup>a</sup>, G. de France<sup>j</sup>, N. Erduran<sup>k</sup>, A. Gadea<sup>d</sup>,  
M. Moszyński<sup>l</sup>, J. Nyberg<sup>m</sup>, M. Palacz<sup>n</sup>, R. Wadsworth<sup>o</sup>, R. Aliaga<sup>d</sup>,  
C. Aufranc<sup>q</sup>, M. Bézard<sup>j</sup>, G. Baulieu<sup>q</sup>, E. Bissiato<sup>a</sup>, A. Boujrad<sup>j</sup>, I. Burrows<sup>p</sup>,  
S. Carturan<sup>a,b</sup>, P. Cocconi<sup>a</sup>, G. Colucci<sup>b,c</sup>, D. Conventi<sup>a</sup>, M. Cordwell<sup>p</sup>,  
S. Coudert<sup>j</sup>, J.M. Deltoro<sup>a</sup>, L. Ducroux<sup>j</sup>, T. Dupasquier<sup>q</sup>, S. Ertürk<sup>r</sup>,  
X. Fabian<sup>q</sup>, V. González<sup>s</sup>, A. Grant<sup>p</sup>, K. Hadyńska-Kleń<sup>a,t</sup>, A. Illana<sup>a</sup>,  
M. L. Jurado-Gomez<sup>d</sup>, M. Kogimtzis<sup>p</sup>, I. Lazarus<sup>p</sup>, L. Legeard<sup>j</sup>, J. Ljungvall<sup>u</sup>,  
G. Pasqualato<sup>b,c</sup>, R. M. Pérez-Vidal<sup>d</sup>, A. Raggio<sup>a</sup>, D. Ralet<sup>j</sup>, N. Redon<sup>q</sup>,  
F. Saillant<sup>j</sup>, B. Saygi<sup>v</sup>, E. Sanchis<sup>s</sup>, M. Scarciuffolo<sup>b,c</sup>, M. Siciliano<sup>a</sup>,  
D. Testov<sup>b,c</sup>, O. Stezowski<sup>q</sup>, M. Tripon<sup>j</sup>, I. Zanon<sup>a</sup>

<sup>a</sup>*Istituto Nazionale di Fisica Nucleare, Laboratori Nazionali di Legnaro, Legnaro, Italy*

<sup>b</sup>*Dipartimento di Fisica e Astronomia, Università di Padova, Padova, Italy*

<sup>c</sup>*Istituto Nazionale di Fisica Nucleare, Sezione di Padova, Università di Padova, Padova, Italy*

<sup>d</sup>*Instituto de Física Corpuscular, CSIC-Universidad de Valencia, E-46980 Paterna (Valencia), Spain*

<sup>e</sup>*Department of Physics, University of Oslo, N-0316 Oslo, Norway*

<sup>f</sup>*CERN, Switzerland*

<sup>g</sup>*Niewodniczanski Institute of Nuclear Physics, Polish Academy of Sciences, Kraków, Poland*

<sup>h</sup>*Extreme Light Infrastructure Nuclear Physics (ELI-NP), 077125 Bucharest-Magurele, Romania*

<sup>i</sup>*Helmholtz Institute Mainz and GSI Helmholtzzentrum für Schwerionenforschung Darmstadt, Germany*

<sup>j</sup>*GANIL, CEA/DRF-CNRS/IN2P3, Bvd. Henri Becquerel, 14076 Caen, France*

<sup>k</sup>*Faculty of Engineering and Natural Sciences, Istanbul Sabahattin Zaim University, 34303 Istanbul, Turkey*

<sup>l</sup>*National Centre for Nuclear Research, 05-400 Otwock-Świerk, Poland*

<sup>m</sup>*Department of Physics and Astronomy, Uppsala University, SE-75120 Uppsala, Sweden*

<sup>n</sup>*Heavy Ion Laboratory, University of Warsaw, 02-093 Warsaw, Poland*

<sup>o</sup>*Department of Physics, University of York, Heslington, YO10 5DD York, U.K.*

<sup>p</sup>*STFC Daresbury Laboratory, Daresbury, Warrington WA4 4AD, U.K.*

<sup>q</sup>*Université Lyon 1, CNRS, IN2P3, IPN Lyon, F-69622 Villeurbanne, France*

<sup>r</sup>*Department of Physics, University of Nigde, 51240 Nigde, Turkey*

<sup>s</sup>*Departamento de Ingeniería Electrónica, Universidad de Valencia. Avda. Universidad s/n 46100 Burjassot, Spain.*

<sup>t</sup>*Department of Physics, University of Surrey, Guildford GU2 7XH, U.K.*

<sup>u</sup>*CSNSM, CNRS, IN2P3, Université Paris-Sud, F-91405 Orsay, France*

<sup>v</sup>*Department of Physics, Faculty of Science, University of Ege, Izmir, 35100, Turkey*

---

## Abstract

The NEutron Detector Array, NEDA, will form the next generation neutron detection system that has been designed to be operated in conjunction with  $\gamma$ -ray arrays, such as the tracking-array AGATA, to aid nuclear spectroscopy studies. NEDA has been designed to be a versatile device, with high-detection efficiency, excellent neutron- $\gamma$  discrimination and high rate capabilities. It will be employed in physics campaigns in order to maximise the scientific output, making use of the different European stable and radioactive ion beams. The

50 first implemenation of the neutron detector array NEDA with AGATA  $1\pi$  was  
51 realized at GANIL. This manuscript reviews the various aspects of NEDA.

52 *Keywords:* NEDA, Nuclear structure, gamma-ray spectroscopy, neutron  
53 detector, liquid scintillator, digital electronics, neutron-gamma discrimination

---

## 54 1. Introduction

55 The main objective of nuclear structure is to study the nature and phe-  
56 nomenology of the nucleon-nucleon interaction in the nuclear medium. Gamma-  
57 ray spectroscopy represents one of the most powerful methods to study nuclear  
58 structure since a large fraction of the de-excitation of the excited nuclear levels  
59 goes via the emission of  $\gamma$  rays. High-resolution  $\gamma$ -ray spectroscopy makes it possible  
60 to perform high precision measurements that help to determine the energy,  
61 angular momentum and parity of nuclear excited states, as well as transition  
62 probabilities using a variety of techniques. All this information characterizes  
63 the nucleus under study. The knowledge of nuclear matter has progressed *pari*  
64 *passu* with the technical development of  $\gamma$ -ray spectrometers and associated ancillary  
65 devices that the nuclear spectroscopy community has built up over the  
66 last five decades.

67 The NEutron Detector Array (NEDA) [1, 2, 3, 4, 5, 6, 7, 8] is a neutron  
68 detector array of the next generation. It has been constructed as an ancillary  
69 detector for use with the Advanced Gamma Tracking Array (AGATA), which is  
70 a state-of-the-art high-resolution  $\gamma$ -ray spectrometer based on the  $\gamma$ -ray tracking  
71 technique [9]. The first implementation of NEDA has been done with AGATA  
72  $1\pi$  at GANIL [1, 10]. However, other large  $\gamma$ -ray arrays are also foreseen to  
73 be coupled to NEDA. Neutron and charged-particle detectors provide a good  
74 selection of the decay channels that has been demonstrated to be very efficient  
75 for the study of neutron-deficient nuclei populated by fusion-evaporation re-  
76 actions, e.g. for the investigation of nuclei close to the  $N=Z$  line. NEDA is  
77 also a well suited device for the investigation of exotic nuclei populated with  
78 transfer reactions, where the emitted particle is a neutron. A large variety of  
79 new radioactive beams will be accessible in the next years for transfer reactions  
80 induced by proton- and neutron-rich projectiles from radioactive beam facilities  
81 such as HIE-ISOLDE (CERN, Geneva, Switzerland), SPES (Legnaro, Italy),  
82 SPIRAL2 (Caen, France) and FAIR (Darmstadt, Germany). Neutron detectors  
83 based on liquid scintillators that provide neutron- $\gamma$  identification by pulse-shape  
84 discrimination and Time-of-Flight (ToF) have been in use for decades. There  
85 are a few examples of high-efficiency neutron detectors with high discrimination  
86 capabilities between neutrons and  $\gamma$  rays that can be coupled to large  $\gamma$ -ray  
87 arrays, such as Neutron Wall [11, 12], Neutron Shell [13] and DESCANT [14].

88 The conceptual design of NEDA is discussed in Section 2. The outcome of  
89 our considerations for a broad use of NEDA in different experimental conditions  
90 yielded a design based on a modular array of hexagonal single detectors that can  
91 tile up a compact surface or a hemisphere, see Section 3. Section 4 describes  
92 the fully-digital front-end electronics conceived to obtain excellent neutron- $\gamma$   
93 discrimination capabilities, integration with fully digital modern  $\gamma$ -ray arrays  
94 and flexibility. Finally, Section 5 discusses the data-acquisition system imple-  
95 mented for NEDA and AGATA.

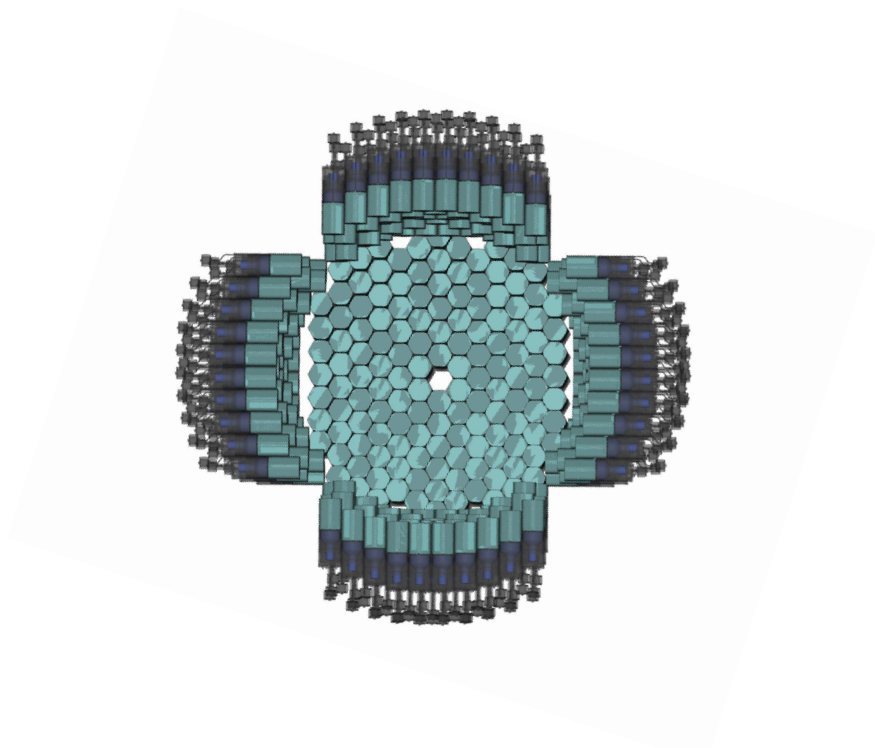


Figure 1: Proposed NEDA geometry for a  $2\pi$  angular coverage at one meter distance. The total number of identical NEDA detectors is 331, covering a solid angle of  $1.88 \pi$  s.r.

## 96 2. Conceptual design

97 NEDA is conceptually designed to be a versatile and a highly-efficient neu-  
 98 tron detector array with good neutron- $\gamma$  discrimination capabilities at high  
 99 counting rates. It will be used as a neutron tagging instrument coupled with  
 100 large  $\gamma$ -ray arrays at stable and radioactive ion beam facilities, that will effi-  
 101 ciently measure neutrons emitted from outgoing channels in fusion-evaporation  
 102 and low-energy transfer reactions. The kinematics of particles emitted in these  
 103 two types of nuclear reactions, fusion-evaporation and transfer, demand very  
 104 different characteristics from a neutron detector. In the former case, the neu-  
 105 trons have a Maxwellian distribution with a maximum at energies of a few  
 106 MeV and due to the kinematics of the reaction, they have an angular distri-  
 107 bution peaked at forward angles with respect to the beam direction. NEDA  
 108 has specially been optimised to have large efficiency in such fusion-evaporation  
 109 reactions, for neutron multiplicities 2 and 3. In transfer reactions, the neutrons  
 110 can reach energies above 10 MeV and their angular distributions highly depend  
 111 on the angular momentum transferred, energy of the beam, and kinematics of  
 112 the reaction.

113 An early implementation of NEDA combined with Neutron Wall and AGATA  
 114 for fusion-evaporation reactions is described in Ref. [1]. In this first usage of  
 115 NEDA, a limited number of NEDA detectors were coupled together with the  
 116 Neutron Wall at approximately half a meter from the target with an angular

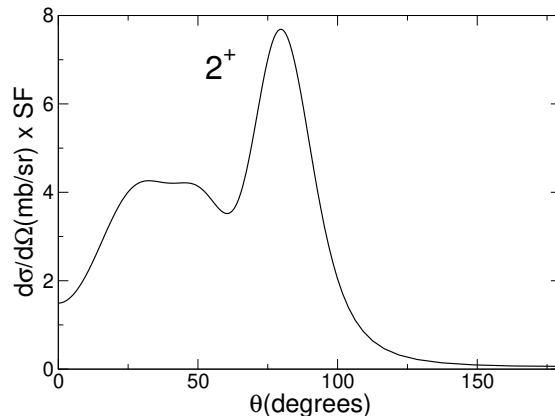


Figure 2: Calculated cross sections for the  $2^+$  state with Twofnr [15] as a function of the angle of the emitted neutrons in the laboratory reference frame for the reaction  ${}^3\text{He}({}^{18}\text{Ne},n){}^{20}\text{Mg}$  at 4.0 MeV $\times$ A. SF is the spectroscopic factor, that has been considered one for this case.

117 coverage of  $1.6 \pi$  s.r. In this reference, a large discussion was dedicated to the  
 118 validation of the GEANT4 simulations with experimental data. Whereas, the  
 119 present work is devoted to a discussion of the NEDA  $2\pi$  configuration, which  
 120 will be composed of 331 single NEDA detectors located one meter from the  
 121 target and covering a solid angle of  $1.88 \pi$  s.r.. The angular coverage for each  
 122 individual detector is about  $7.5^\circ$ . This configuration will allow for an improve-  
 123 ment of not only neutron- $\gamma$  discrimination, based on Time-Of-Flight (TOF)  
 124 measurements but also the neutron angular resolution, which is essential for  
 125 measuring, in transfer reactions, the angular momentum transferred. The ge-  
 126 ometry for the NEDA  $2\pi$  configuration at one meter focal distance is shown  
 127 in Fig. 1. Simulations for this geometry were performed by using the previ-  
 128 ously developed event generator for GEANT4 simulations, producing neutrons  
 129 emitted by a  ${}^{252}\text{Cf}$  source and in the fusion-evaporation reaction  ${}^{58}\text{Ni} + {}^{56}\text{Fe}$   
 130 at 220 MeV [1]. In addition, a possible future transfer reaction to be used  
 131 with NEDA has been considered in the simulations, namely  ${}^3\text{He}({}^{18}\text{Ne},n){}^{20}\text{Mg}$   
 132 at 4.0 MeV $\times$ A. For this latter case an isotropic angular distribution as well  
 133 as a realistic angular distribution for the neutrons, calculated with the DWBA  
 134 Twofnr code [15], has been used as the event-generator input for the GEANT4  
 135 simulations. The flat angular distribution is purely an academic exercise, where  
 136 the important parameter that will affect the efficiencies is the neutron energy.  
 137 Figure 2 shows the calculated cross sections for the  $2^+$  state as a function of the  
 138 angle of the emitted neutron in the laboratory reference frame.

139 Table 1 shows the simulated one-, two- and three-neutron detection efficien-  
 140 cies for emissions from a  ${}^{252}\text{Cf}$  (*Cf*) source and from the fusion-evaporation  
 141 reaction  ${}^{58}\text{Ni} + {}^{56}\text{Fe}$  at 220 MeV (*FE*) for a light threshold of 50 keVee. The  
 142 one-neutron efficiency obtained for the transfer reaction  ${}^3\text{He}({}^{18}\text{Ne},n){}^{20}\text{Mg}$  at  
 143 4.0 MeV per nucleon is also shown. A full angular dependence (*TA*) and a flat  
 144 distribution (*TF*) have been considered for this physics case. For this study  
 145 cases (*TA* and *TF*), the neutrons have an energy of 17 MeV at zero degrees  
 146 and around 3 MeV at ninety degrees. The simulation that considers the real  
 147 angular distribution will reflect, in addition to the efficiency for the large energy  
 148 neutrons, the angular integrated cross-section which is very much dependent

Table 1: One-, two- and three-neutron detection efficiencies obtained from simulations of a  $^{252}\text{Cf}$  source (*Cf*) and the fusion-evaporation reaction,  $^{58}\text{Ni}$  (220 MeV) +  $^{56}\text{Fe}$  (*FE*). The one-neutron efficiency, simulated for the transfer reaction  $^3\text{He}(^{18}\text{Ne},\text{n})^{20}\text{Mg}$  at 4.0 MeV per nucleon, is also shown. For this case a full angular dependence (*TA*) and an isotropic distribution of the emitted neutron (*TF*) have been considered. The final values of the efficiencies have been scaled by the correction factor discussed in Ref. [1]. Results obtained for a light threshold of 50 keVee. Errors quoted are statistical.

| Geometry         | $\varepsilon_{1\text{n}}$ [%] | $\varepsilon_{2\text{n}}$ [%] | $\varepsilon_{3\text{n}}$ [%] |
|------------------|-------------------------------|-------------------------------|-------------------------------|
| NEDA $2\pi$ - Cf | 23.82(15)                     | 4.33(7)                       | 0.63(3)                       |
| NEDA $2\pi$ - FE | 40.54(7)                      | 11.49(9)                      | 3.7(2)                        |
| NEDA $2\pi$ - TA | 42.75(7)                      | -                             | -                             |
| NEDA $2\pi$ - TF | 18.67(4)                      | -                             | -                             |

149 on each specific beam and target combination, the angular momentum transferred and the energy of the beam. The simulations of the NEDA  $2\pi$  version  
150 at one meter focal distance can not be directly compared to the results presented in Ref. [1] since in the present simulation a 50 keVee threshold has been  
151 utilised, whereas the simulations presented in Ref. [1] were performed with a threshold of 150 keVee for the NEDA detectors and an individual threshold for  
152 each Neutron Wall detector. For transfer reactions were high energy neutrons are involved the full NEDA array still keeps a large efficiency as can be seen  
153 in Table 1 for the case of a isotropic angular distribution. This is because the NEDA detectors have a significant intrinsic neutron detection efficiency due to  
154 their depth of around 20 cm. In addition to the large efficiency of the NEDA  $2\pi$  at one meter focal distance, one should consider other aspects: among those  
155 aspects it is worth noticing that by exploiting the larger flight path it will be possible to improve the neutron- $\gamma$  discrimination and the energy resolution, due  
156 to the longer TOF, as well as the angular resolution, due to the smaller solid angles subtended by each single detector.  
157  
158  
159  
160  
161  
162  
163  
164

### 165 3. Detectors

166 The single NEDA detector was carefully designed in order to achieve the best possible efficiency, time resolution, neutron- $\gamma$  discrimination and minimise cross-talk among detectors. Extensive Monte Carlo simulations were carried out to optimise the type of scintillator used, the size of a single detector and its distance to the target and thus the granularity of the array [2]. The final decision was to build individual NEDA detectors with a cross-section fitting a 5 inch Photo Multiplier Tube (PMT) with a length of around 20 cm. The active volume of the detector was filled with the liquid scintillator ELJEN EJ301 (which is equivalent to BC501A). Furthermore, since a highly efficient array was foreseen, a fully tiled up surface was required, with minimum dead layers in between. Only three regular polygons (square, triangle, hexagon) can tile a flat surface without gaps. This can be done by using only one type of these polygons or a combination of several of them. One of the polygons, the regular hexagon, was chosen as the starting point for the NEDA geometry since its profile covers the largest fraction of the area of a photomultiplier with a circular cross section.

181 A single NEDA detector is shown in Fig. 3. The detector cell is made of  
182 6060 aluminium alloy and has a hexagonal profile with a 146 mm side to side  
183 distance, and 3 mm thick walls. It is 205 mm long, with an active volume of

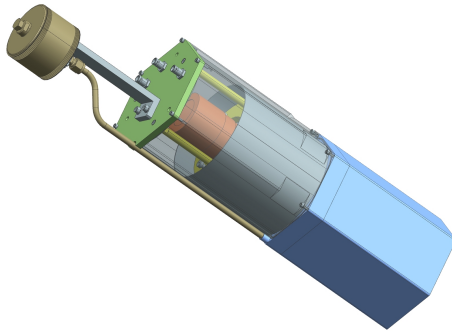


Figure 3: Drawing showing the design of a NEDA neutron detector. It has a hexagonal profile with a cell (blue) where the liquid organic scintillator EJ301 is placed. This cell is connected via a pipe to an expansion bellow (brown). A hexagonal light tight casing contains the Photo Multiplier Tube and voltage divider (orange) as well as a mu-metal shielding (grey). The spring pusher for the PMT is shown in yellow.

184  $\sim 3.15$  litres filled with the liquid organic scintillator EJ301. The inner surface  
 185 is coated with  $\text{TiO}_2$ -based reflective paint EJ520. The top flange includes a 5  
 186 inch N-BK7 5 mm thick glass window, which has 92% transmittance for the  
 187 wavelength spectrum emitted by the scintillator. A pipe connects the active  
 188 volume of the detector with an expansion chamber located on the top of the  
 189 PMT casing. This expansion chamber is needed to allow for the change in  
 190 volume of the scintillator with temperature. The edge welded bellow (expansion  
 191 chamber) is 3 inch in diameter and expands up to  $153 \text{ cm}^3$  in a stroke of 4.8 cm,  
 192 leading to an operational temperature range of  $40^\circ\text{C}$  with minimal pressure  
 193 differences. The design of a single NEDA detector has been already described  
 194 in Ref. [16].

195 An investigation into the best possible PMT existing in the market that  
 196 would provide good neutron- $\gamma$  discrimination, as well as the best possible tim-  
 197 ing, was performed and published in Ref. [3]. From the various PMTs on the  
 198 market (ET9390-kb produced by ET Enterprises and the Hamamatsu R4144  
 199 and R11833-100), it was shown that ET9390-kb and R11833-100 are of simi-  
 200 lar quality giving a Figure Of Merit (FOM), as defined in Ref. [17] of  $\approx 1.7$   
 201 at  $320 \pm 20$  keVee for a commercial test detector, which was significantly better  
 202 than R4144. Taking into account also the timing properties of the three PMTs,  
 203 thoroughly discussed in Ref. [4], the final choice was the Hamamatsu PMT of  
 204 model R11833-100 with a super bialkali photocathode. The voltage divider,  
 205 designed and constructed within the collaboration for the R11833-100 PMT, is  
 206 transistorised in order to sustain large counting rates without loosing linearity.  
 207 Successful linearity tests were performed up to counting rates of  $\sim 300$  kHz.

208 The final detector, which is self produced by the NEDA collaboration, has  
 209 an excellent light yield of  $2850 \pm 100$  photoelectrons per MeVee. The average  
 210 value is almost a factor of two larger than what was obtained for the previously  
 211 developed detectors for the EUROBALL Neutron Wall [11]. Figure 4 shows a  
 212 typical neutron- $\gamma$  discrimination, based on the charge comparison method [17],  
 213 as a function of light yield in keVee measured with a  $^{252}\text{Cf}$  source. One can  
 214 note, the excellent separation of the  $\gamma$  and neutron distributions even for such  
 215 large scintillator volume.

216 Further detailed information on the design, construction, tests and perfor-  
 217 mance of a single NEDA detector will be provided in a forthcoming publica-  
 218 tion [18].

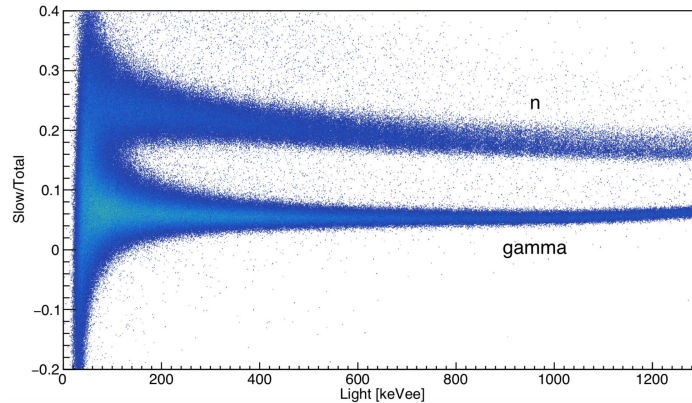


Figure 4: Pulse-shape discrimination based on the charge comparison method [17] measured with a NEDA detector using a  $^{252}\text{Cf}$  source. The ratio of the light in the slow component of the digitised signal divided by the total light is shown on the y axis as a function of the total light in keVee on the x axis.

#### 219 4. Front-end electronics

220 NEDA Front-End Electronics (FEE), unlike its predecessor the Neutron  
 221 Wall, is fully-digital and envisaged to improve the neutron- $\gamma$  discrimination,  
 222 as well as the processing capabilities, integration and overall flexibility [5]. As  
 223 mentioned before, NEDA is primarily designed to be used together with various  
 224 Ge detector systems, in particular with AGATA, EXOGAM2 [19, 20] and the  
 225 GALILEO [21] arrays. In order to facilitate this coupling, the electronics of  
 226 NEDA uses the Global Trigger and Synchronisation (GTS) system [22].

227 The detector photomultiplier tube delivers a current signal through a 15-  
 228 m-long shielded coaxial cable to a NIM module that provides the Single-Ended  
 229 to DIFFerential (SE-DIFF) conversion. SE-DIFF delivers differential analog  
 230 signals to the digitizers and pre-processing modules by means of HDMI cab-  
 231 les. These two sets of cables have been selected carefully to cope with the sig-  
 232 nal bandwidth and crosstalk performance requirements of NEDA. The shielded  
 233 coaxial 15-m cables have a -0.43 dB @ 480 MHz. While the 1.5-m HDMI cables  
 234 have a bandwidth of 430 MHz and crosstalk levels of -42.29/-48.11 dB for signals  
 235 with rise-times of 3 and 7 ns, respectively.

236 The SE-DIFF module has been developed in the NIM standard and contains  
 237 a PCB board capable of converting the signals of 16 detectors. The board uses  
 238 a fully-differential amplifier AD8139 and each channel is adapted to work in a  
 239 range of 3 V, although the input range can be increased up to 8 V, activating a  
 240 voltage divider available at the input stage.

241 The core of the FEE is the NUMEXO-2 cards developed for EXOGAM2,  
 242 which consist of a set of 4 Flash Analog-to-Digital-Converter (FADC) Mezza-  
 243 nines in charge of digitising the signals at 200 Msps. The FADC mezzanines



244 contain each four Analog-to-Digital (A/D) modules. In addition, the cards con-  
 245 tain a motherboard which includes two large FPGAs used to perform the trigger  
 246 generation, digital signal processing, clocking, data packaging and readout tasks  
 247 to the servers for 16 independent channels.

248 The FADC Mezzanine is the daughterboard in charge of the A/D conversion,  
 249 whose sampling frequency and resolution specifications have been selected on  
 250 the basis of the signal properties to be digitised [6, 7]. These specifications  
 251 do not come only from the NEDA project since the FADC Mezzanines were  
 252 also designed for other projects such as EXOGAM2. The major resolution  
 253 constraint comes from the EXOGAM side whose specification of 2.3 keV @  
 254 1.33 MeV led to a choice of an ADC with ENOB > 11.3. To fulfil the various  
 255 needs of NEDA and EXOGAM2 the final choice was to use the ADS62P49  
 256 sampling device, providing a board with 4 channels sampling at 200 Msp/s with  
 257 an ENOB of 11.6-11.7 bits. As for the clock, the main 100 MHz clock from  
 258 the GTS is obtained, and processed with a jitter cleaner in order to produce  
 259 a 200 MHz sampling clock. At the input of the FADC Mezzanine, an analog  
 260 fully-differential coupling stage adapts the input range to the ADC chip range,  
 261 with the added capability of a controllable offset which permits use of the full  
 262 FADC dynamics.

263 The NUMEXO-2 motherboard includes two FPGAs, a Virtex-6 and a Virtex-  
 264 5, which carry out the pre-processing tasks. The Virtex-6 FPGA performs the  
 265 data processing, trigger elaboration, package building and formatting, whereas  
 266 the Virtex-5 FPGA manages the readout via PCIe, slow control via Ethernet,  
 267 integration of the GTS leaf and implementation of the ADC interface, which is  
 268 the block in charge of storing temporarily the data before validation by the GTS  
 269 system. A descriptive view of how the blocks are structured inside the FPGA  
 270 is depicted in Fig. 5. In the following paragraphs the functionalities included in  
 271 the two NUMEXO-2 FPGAs will be discussed.

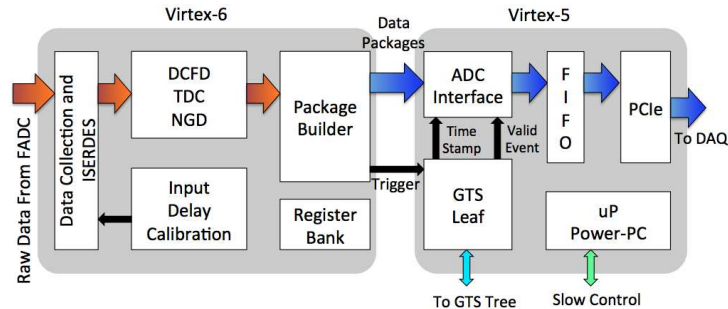


Figure 5: Block diagram depicting the main blocks in the NUMEXO-2 as well as the interaction among them.

272 The first block found at the beginning of the Virtex-6 is a customized ar-  
 273 rangement of serialization/deserialization sub-blocks (called ISERDES), used  
 274 to convert the multiplexed bit pairs provided from the FADCs into process-  
 275 able samples. After that, the first component that the data finds is a baseline  
 276 cancellation block and a first-level local trigger based either on a leading edge  
 277 or a Digital Constant Fraction Discriminator (DCFD). The first-level trigger  
 278 enables a Pulse Shape Analysis (PSA) for neutron- $\gamma$  discrimination based on

279 the charge-comparison method [17], that will provide the Trigger Request used  
280 in the GTS Validation/Rejection cycle [22]. Note that, for this block, param-  
281 eters such as the fast and slow signal component integration times, as well as  
282 the discrimination threshold, are programmable. In parallel, a Time-of-Flight  
283 evaluation is done with a TDC process in the FPGA, calculating the time be-  
284 tween the DCFD zero-crossover signal and an external reference signal, which  
285 is normally provided by the accelerator. The Trigger Request could be also  
286 generated by a time condition on the TDC result and can be combined with  
287 the PSA Trigger Request with boolean AND or OR conditions. Eight LVDS  
288 data lanes communicating with both FPGAs at rates up to 400 MB/s allow  
289 a sustained counting rate of 20 kHz trigger request in the 16 channels present  
290 in the NUMEXO-2 board. The data frames created in the Virtex-6 FPGA are  
291 compatible with the MFM GANIL data format specification. As mentioned  
292 in the previous sub-section, the GTS standard has been chosen for NEDA. A  
293 specific implementation of the GTS leaf, supporting the 16 Trigger Request of a  
294 NEDA NUMEXO-2 board, has been implemented in the Virtex-5 FPGA. The  
295 ADC interface process stores temporarily the data buffers and waits for the GTS  
296 validation prior to sending the evaluated and sample data information via the  
297 PCIe interface. NEDA uses the NUMEXO-2 4x PCIe v1.0 Endpoint link to read  
298 out the data. The data are sent to a server (one server per NUMEXO-2) via  
299 an MPO optical fibre. On the receiver side, a commercial PCIe bridge card is  
300 hosted in the server and converts the optical input to the PCIe legacy bus stan-  
301 dard. The Virtex-5 FPGA includes a PowerPC (PPC) 440 processor, running  
302 an embedded Linux OS, that manages the slow control and GTS services.

## 303 5. Data acquisition

304 In its first implementation at GANIL, the array was used together with  
305 AGATA, DIAMANT [23] and the Neutron Wall. In this setup, a total of 54  
306 NEDA detectors and 42 Neutron Wall detectors were used. The signals from  
307 the 96 neutron detectors were digitised by six NUMEXO-2 cards. In order to  
308 ensure compatibility of the data acquisition systems of NEDA and AGATA, the  
309 choice was made to base the data acquisition on the NARVAL system. This sys-  
310 tem, developed by IPN Orsay, uses the ADA language to manage the data flux  
311 through several steps from the producer receiving the data from the electronics  
312 down to the event reconstruction and merging of NEDA data together with the  
313 AGATA and DIAMANT data. The architecture of the acquisition system for  
314 one NUMEXO-2 board is presented in Fig. 6. The transmission of the data  
315 between the different actors is integrated in the NARVAL system and based on  
316 the TCP/IP and InfiniBand protocols for actors located on separated servers,  
317 or UNIX FIFO for actors on the same server. Thanks to the flexibility of the  
318 NARVAL system C++ actors developed, within the AGATA-NEDA collabora-  
319 tion, are in charge of the data treatment and can be integrated through shared  
320 libraries loaded in the NARVAL environment.

321 In Section 4, it was shown that the slow-control and the alignment of the  
322 GTS system is controlled through the ethernet. To ensure the time alignment  
323 of the GTS of NEDA and AGATA, the NUMEXO-2 boards are inserted in a  
324 sub-network of the AGATA electronics network. The data transfer of the raw  
325 events corresponding to a header containing the channel identification and tim-  
326 ing information is made through a dedicated optical link. Thus, each of the 6

327 NUMEXO-2 boards necessary to accommodate the 96 channels of the NEDA-  
 328 NeutronWall array, plus one spare board, are optically connected to dedicated  
 329 servers in charge of the data pre-processing. Commercial PCI-express optical  
 330 bridges from Samtec are used to make the link between the NUMEXO-2 digitiz-  
 331 ers and the servers. After this optical transmission, the processed data transit  
 332 through two different networks: the GANIL network, where all the local pro-  
 333 cessing of the data and the storage of the raw events is done and the AGATA  
 334 network, on which the two data (NEDA and AGATA) sets are combined. A  
 335 schematic view of the data acquisition system is shown in Fig. 6.

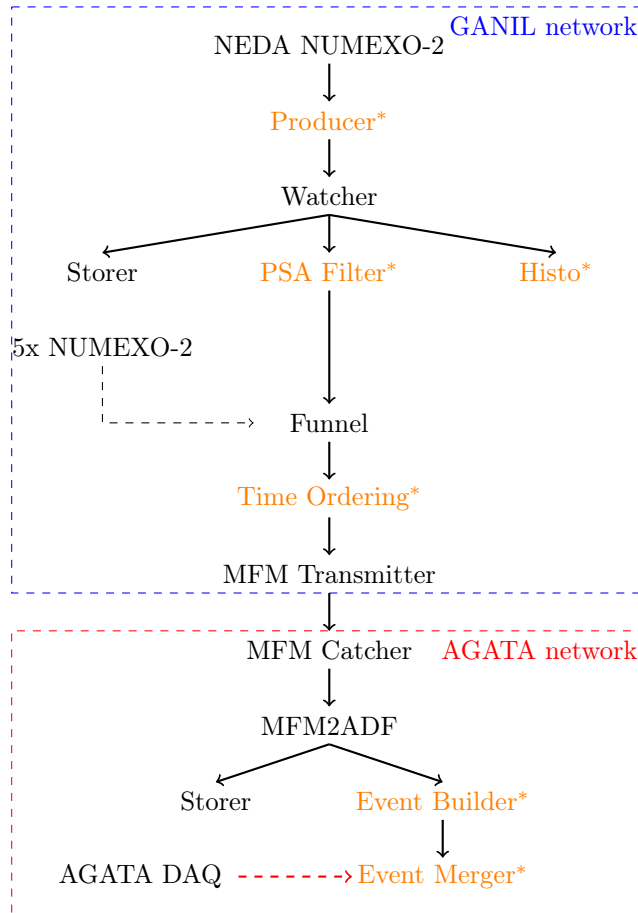


Figure 6: Schematic view of the NEDA data acquisition system. The actors marked with an asterisk are actors developed in C++ within the collaboration. The other actors are standard NARVAL actors. The NEDA acquisition system is shared between two networks: the GANIL and the AGATA network. The transmission of the data between the two networks is performed by one bridge.

336 A dedicated C++ actor, called Producer in Fig. 6, has been developed to  
 337 extract the events from the Direct Memory Access (DMA) and transmit them  
 338 into the NARVAL environment. The data are then transmitted to a standard  
 339 actor which is in charge of copying the data to three different branches and  
 340 sending them to three actors: i) a storer, which is used to remotely store the

341 full events with the captured traces (digitised signals) on disk that allows for  
342 reprocessing the events offline with advanced PSA algorithms such as a Neural  
343 Network (NN) [24, 25], ii) a histogrammer, indicated by Histo in Fig. 6, for data  
344 quality monitoring, and, finally, iii) an online PSA code.

345 Three different algorithms have been implemented in the PSA Filter: a  
346 Charge-Comparison (CC) algorithm, similar to the one used at the FPGA level,  
347 an integrated rise-time algorithm and finally the Neural Network algorithm de-  
348 scribed in Ref. [25]. In order to limit the quantity of data transmitted on the  
349 network, the choice was made to discard the traces at the output of the PSA  
350 filter. The reduced frame, containing only the parameters out of the pulse shape  
351 algorithms and the frame header are transmitted though Ethernet to a server,  
352 where a NARVAL actor concatenates the data from the 6 servers into a single  
353 output transmitted to a time ordering filter. This stage of time ordering is es-  
354 sential as the Funnel in Fig. 6 only loops over the 6 inputs and passes the input  
355 buffers in the order of the input branches. It is also for this reason, that the  
356 detectors are distributed over the different boards in a pie like configuration in  
357 order to distribute the counting rate on each of them as equally as possible. It is  
358 only after the time sorting that the data are transmitted frame-by-frame to the  
359 AGATA acquisition system, in a manner similar to that used for the VAMOS++  
360 campaign [10], namely by using the MFMTransmitter and MFMCatcher actors.  
361 Once in the AGATA world, the MFM frames are encapsulated into AGATA  
362 Data Format (ADF) frames using a dedicated key. In order to make the replay  
363 of the data faster, a storer is implemented at the output of this actor. Indeed,  
364 this allows offline building of the NEDA events directly in the AGATA world  
365 without having to do a full PSA analysis of the traces. Before merging the  
366 NEDA and AGATA data together, the NEDA events are reconstructed in order  
367 to extract the real neutron multiplicity using neutron scattering algorithms.

## 368 6. Summary

369 The NEutron Detector Array, NEDA, has been designed to be a versatile  
370 device, with high detection efficiency, excellent neutron- $\gamma$  discrimination and  
371 high count rate capabilities. NEDA will be used together with large  $\gamma$ -ray  
372 arrays at stable and radioactive beam facilities such as HIE-ISOLDE (CERN,  
373 Geneva, Switzerland), LNL/SPES (Legnaro, Italy), GANIL/SPIRAL2 (Caen,  
374 France) and FAIR (Darmstadt, Germany). The physics challenges that NEDA  
375 will be facing in the near future will be the study of neutron-deficient nuclei  
376 populated with fusion-evaporation reactions, close to  $N=Z$  as well as transfer  
377 studies where the emitted particles are neutrons. NEDA will be comprised of  
378 331 detectors, filled with EJ301 liquid scintillator, where each single detector has  
379 an hexagonal profile that allows for a fully tiled up surface. The detector cross-  
380 section fits a 5 inch Photo Multiplier Tube (PMT) and it has a length of around  
381 20 cm. A photomultiplier with a super bialkali photocathode (R11833-100) and  
382 a transistorised voltage divider to sustain large counting rates are used for the  
383 read out. The detectors, which are self-made by the NEDA collaboration, have  
384 excellent neutron- $\gamma$  discrimination and timing properties. The NEDA front-  
385 end electronics is fully digital and uses the Global Trigger and Synchronisation  
386 system to improve processing capabilities, flexibility and integration with other  
387 detector systems, in particular  $\gamma$ -ray arrays such as AGATA. The core of the  
388 front-end electronics are the NUMEXO-2 cards that consist of a set of four

389 FADC Mezzanines, each containing four 200 Msps digitisers. The motherboards  
390 of the cards contain two FPGA units, a Virtex-6 and a Virtex-5, which carry  
391 out the pre-processing tasks. The data acquisition system of NEDA in its first  
392 implementation with AGATA is based on the NARVAL system.

## 393 7. Acknowledgements

394 This study is supported by the Swedish Research Council (contract number  
395 VR 2014-6644), the Scientific and Technological Research Council of Turkey  
396 (TUBITAK Project No: 117F114), the Polish National Science Centre, grants  
397 nos. 2017/25/B/ST2/01569 and 2016/22/M/ST2/00269 COPIN-IN2P3 and  
398 COPIGAL projects, the UK STFC under grant nos. (ST/J000124/1, ST/L005727/1,  
399 STL005735/1, ST/P003885/1), the Generalitat Valenciana and MICIU, Spain,  
400 grants PROMETEO II/2014/019, FPA2017-84756-C4, Severo Ochoa SEV-2014-  
401 0398 and and by the E.C. FEDER funds.

## 402 References

- 403 [1] T. Hüyük, A. Di Nitto, G. Jaworski, A. Gadea, J. J. Valiente-Dobón, J. Ny-  
404 berg, M. Palacz, P.-A. Söderström, R. J. Aliaga-Varea, G. de Angelis, et al.,  
405 Conceptual design of the early implementation of the neutron detector ar-  
406 ray (neda) with agata, *The European Physical Journal A* 52 (3) (2016)  
407 1–8.
- 408 [2] G. Jaworski, M. Palacz, J. Nyberg, G. De Angelis, G. De France,  
409 A. Di Nitto, J. Egea, M. Erduran, S. Ertürk, E. Farnea, et al., Monte carlo  
410 simulation of a single detector unit for the neutron detector array neda,  
411 *Nuclear Instruments and Methods in Physics Research Section A: Accel-  
412 erators, Spectrometers, Detectors and Associated Equipment* 673 (2012)  
413 64–72.
- 414 [3] X. Luo, V. Modamio, J. Nyberg, J. Valiente-Dobón, Q. Nishada, G. De An-  
415 gelis, J. Agramunt, F. Egea, M. Erduran, S. Ertürk, et al., Test of digital  
416 neutron–gamma discrimination with four different photomultiplier tubes  
417 for the neutron detector array (neda), *Nuclear Instruments and Methods  
418 in Physics Research Section A: Accelerators, Spectrometers, Detectors and  
419 Associated Equipment* 767 (2014) 83–91.
- 420 [4] V. Modamio, J. Valiente-Dobón, G. Jaworski, T. Hüyük, A. Triossi,  
421 J. Egea, A. Di Nitto, P.-A. Söderström, J. A. Ros, G. De Angelis, et al.,  
422 Digital pulse-timing technique for the neutron detector array neda, *Nu-  
423 clear Instruments and Methods in Physics Research Section A: Accelera-  
424 tors, Spectrometers, Detectors and Associated Equipment* 775 (2015) 71–  
425 76.
- 426 [5] F. E. Canet, V. González, M. Tripon, M. Jastrzab, A. Triossi, A. Gadea,  
427 G. De France, J. Valiente-Dobón, D. Barrientos, E. Sanchis, et al., Digital  
428 front-end electronics for the neutron detector neda, *IEEE Transactions on  
429 Nuclear Science* 62 (3) (2015) 1063–1069.

- 430 [6] F. E. Canet, V. González, M. Tripon, M. Jastrzab, A. Triossi, A. Gadea,  
431 G. De France, J. Valiente-Dobón, D. Barrientos, E. Sanchis, et al., A new  
432 front-end high-resolution sampling board for the new-generation electronics  
433 of exogam2 and neda detectors, *IEEE Transactions on Nuclear Science*  
434 62 (3) (2015) 1056–1062.
- 435 [7] F. J. Egea, E. Sanchis, V. González, A. Gadea, J. M. Blasco, D. Barri-  
436 entos, J. V. Dobón, M. Tripon, A. Boujrad, C. Houarner, et al., Design  
437 and test of a high-speed flash adc mezzanine card for high-resolution and  
438 timing performance in nuclear structure experiments, *IEEE Transactions*  
439 *on Nuclear Science* 60 (5) (2013) 3526–3531.
- 440 [8] X. L. Luo, V. Modamio, J. Nyberg, J. J. Valiente-Dobon, Q. Nishada,  
441 G. De Angelis, J. Agramunt, F. J. Egea, M. N. Erduran, S. Erturk,  
442 G. De France, A. Gadea, V. González, A. Goasduff, T. Hüyük, G. Ja-  
443 worski, M. Moszyński, A. Di Nitto, M. Palacz, P.-A. Söderström, E. San-  
444 chis, A. Triossi, R. Wadsworth, Pulse pile-up identification and reconstruc-  
445 tion for liquid scintillator based neutron detectors, *Nuclear Inst. and Meth-*  
446 *ods in Physics Research*, A 897 (2018) 59–65.
- 447 [9] S. Akkoyun, A. Algora, B. Alikhani, F. Ameil, G. De Angelis, L. Arnold,  
448 A. Astier, A. Atac, Y. Aubert, C. Aufranc, et al., Agata: advanced gamma  
449 tracking array, *Nuclear Instruments and Methods in Physics Research Sec-*  
450 *tion A: Accelerators, Spectrometers, Detectors and Associated Equipment*  
451 668 (2012) 26–58.
- 452 [10] E. Clément, C. Michelagnoli, G. de France, H. Li, A. Lemasson, C. B. De-  
453 jean, M. Beuzard, P. Bougault, J. Cacitti, J.-L. Foucher, et al., Conceptual  
454 design of the agata  $1\pi$  array at ganil, *Nuclear Instruments and Methods*  
455 *in Physics Research Section A: Accelerators, Spectrometers, Detectors and*  
456 *Associated Equipment* 855 (2017) 1–12.
- 457 [11] Ö. Skeppstedt, H. Roth, L. Lindström, R. Wadsworth, I. Hibbert, N. Kel-  
458 sall, D. Jenkins, H. Grawe, M. Górska, M. Moszyński, et al., The euroball  
459 neutron wall—design and performance tests of neutron detectors, *Nuclear In-*  
460 *struments and Methods in Physics Research Section A: Accelerators, Spec-*  
461 *trometers, Detectors and Associated Equipment* 421 (3) (1999) 531–541.
- 462 [12] J. Ljungvall, M. Palacz, J. Nyberg, Monte carlo simulations of the neutron  
463 wall detector system, *Nuclear Instruments and Methods in Physics Re-*  
464 *search Section A: Accelerators, Spectrometers, Detectors and Associated*  
465 *Equipment* 528 (3) (2004) 741–762.
- 466 [13] D. Sarantites, W. Reviol, C. Chiara, R. Charity, L. Sobotka, M. Devlin,  
467 M. Furlotti, O. Pechenaya, J. Elson, P. Hausladen, et al., Neutron shell:  
468 a high efficiency array of neutron detectors for  $\gamma$ -ray spectroscopic studies  
469 with gammasphere, *Nuclear Instruments and Methods in Physics Research*  
470 *Section A: Accelerators, Spectrometers, Detectors and Associated Equip-*  
471 *ment* 530 (3) (2004) 473–492.
- 472 [14] P. E. Garrett, DESCANT – the deuterated scintillator array for neutron  
473 tagging, *Hyperfine Interactions* 225 (1-3) (2013) 137–141.

- 474 [15] M. Igarashi, J. Tostevin, Computer Program TWOFNR (Surrey University  
475 version), private communication.
- 476 [16] V. Modamio, et al., First Prototype of the NEDA detector array, INFN-  
477 LNL Annual Report (241).
- 478 [17] P.-A. Söderström, J. Nyberg, R. Wolters, Digital pulse-shape discrimina-  
479 tion of fast neutrons and rays, Nuclear Instruments and Methods in Physics  
480 Research Section A: Accelerators, Spectrometers, Detectors and Associated  
481 Equipment 594 (1) (2008) 79–89.
- 482 [18] G. Jaworski, et al.
- 483 [19] G. De France, EXOGAM: A  $\gamma$ -ray spectrometer for exotic beams, in: Ex-  
484 otic nuclei and atomic masses (ENAM 98). AIP Conference Proceedings,  
485 GANIL, BP 5027, 14076 Coen Cedex 5, France, 1998, pp. 977–980.
- 486 [20] S. L. Shepherd, P. J. Nolan, D. M. Cullen, D. Appelbe, J. Simpson, J. Gerl,  
487 M. Kaspar, A. Kleinboehl, I. Peter, M. Rejmund, H. Schaffner, C. Schlegel,  
488 G. De France, Measurements on a prototype segmented Clover detector,  
489 Nuclear Instruments and Methods in Physics Research Section A 434 (2)  
490 (1999) 373–386.
- 491 [21] J. Valiente-Dobón, et al., Status of the Gamma-Ray Spectrometer  
492 GALILEO, INFN-LNL Annual Report (95).
- 493 [22] M. Bellato, D. Bortolato, J. Chavas, R. Isocrate, G. Rampazzo, A. Triossi,  
494 D. Bazzacco, D. Mengoni, F. Recchia, Sub-nanosecond clock synchroniza-  
495 tion and trigger management in the nuclear physics experiment AGATA,  
496 Journal Of Instrumentation 8 (07) (2013) P07003–P07003.
- 497 [23] J.-N. Scheurer, M. Aiche, M. M. Aléonard, G. Barreau, F. Bourguine,  
498 D. Boivin, D. Cabaussel, J. F. Chemin, T. P. Doan, J. P. Goudour,  
499 M. Harston, A. Brondi, G. La Rana, R. Moro, E. Vardaci, D. Curien,  
500 Improvements in the in-beam  $\gamma$ -ray spectroscopy provided by an ancillary  
501 detector coupled to a Ge  $\gamma$ -spectrometer: the DIAMANT-EUROGAM II  
502 example, Nuclear Instruments and Methods in Physics Research Section A:  
503 Accelerators, Spectrometers, Detectors and Associated Equipment 385 (3)  
504 (1997) 501–510.
- 505 [24] E. Ronchi, P.-A. Söderström, J. Nyberg, E. A. Sundén, S. Conroy, G. Ericson,  
506 C. Hellesen, M. G. Johnson, M. Weiszflog, An artificial neural network  
507 based neutron–gamma discrimination and pile-up rejection framework for  
508 the BC-501 liquid scintillation detector, Nuclear Instruments and Methods  
509 in Physics Research Section A: Accelerators, Spectrometers, Detectors and  
510 Associated Equipment 610 (2) (2009) 534–539.
- 511 [25] P.-A. Söderström, et al., Neutron detection and  $\gamma$ -ray rejection using ar-  
512 tificial neural networks with the liquid scintillators BC-501A and BC-537,  
513 Nuclear Instruments and Methods in Physics Research Section A: Accelerators,  
514 Spectrometers, Detectors and Associated Equipment to be submitted.